Toward the fabrication of extruded microstructured bioresorbable phosphate glass optical fibers

Toward the fabrication of extruded microstructured bioresorbable phosphate glass optical fibers

D. Gallichi-Nottiani[1], D. Pugliese[1], N. G. Boetti[2], D. Milanese[3], D. Janner[1*]

[1]Dipartimento di Scienza Applicata e Tecnologia (DISAT) and RU INSTM, Politecnico di Torino, Corso Duca degli Abruzzi 24, 10129 Torino, Italy

[2]Fondazione LINKS-Leading Innovation and Knowledge for Society, via P. C. Boggio 61, 10138 Torino, Italy

[3]Dipartimento di Ingegneria e Architettura (DIA) and RU INSTM, Università di Parma, Parco Area delle Scienze 181/A, 43124 Parma, Italy

*** Corresponding author:** davide.janner@polito.it

Abstract

The steps toward the fabrication of directly-extruded microstructured fiber preforms made of a bioresorbable phosphate glass are herein presented, analyzing the features of the process from the glass synthesis to the manufacturing of the fiber. The realization of these fibers leverages on three main pillars: an optically transparent bioresorbable glass, its extrusion into a preform and the fiber drawing. The glass has been designed and carefully prepared in our laboratory to be dissolvable in a biological fluid while being optically transparent and suitable for both preform extrusion and fiber drawing. To support the production of an optimized die for the preform extrusion, a simplified laminar flow model simulation has been employed. This model is intended as a tool for a fast and reliable way to catch the complex behavior of glass flow during each extrusion and can be regarded as an effective design guide for the dies to fulfill specific needs for preform fabrication. After die optimization, extrusion of a capillary was realized, and a stacking of extruded tubes was drawn to produce a microstructured optical fiber made of bioresorbable phosphate glass.

Introduction

Phosphate glasses are widely used materials in several fields ranging from optoelectronics to biomedicine. In optoelectronic applications, phosphate glass systems are of great interest due to their broad optical transmission window and high composition flexibility, in particular in terms of high rare-earth ions solubility for lasers.[1,2] In the biomedical field, glasses with different compositions are employed for various applications.[3] Among them, calcium-phosphate glasses have already gained a well-established position especially as a scaffold in both soft and hard tissue engineering.[4–12] Recently, the authors proposed a formulation of calcium-phosphate glass that was drawable in the form of fiber and optically transparent from the Ultraviolet (UV) to the Near-Infrared (NIR).[13] This was achieved by carefully selecting the reagents for glass production to obtain a bioresorbable material (i.e. dissolvable in a biological fluid) that could be cast in a fiber preform and then drawn with the rod-in-tube technique in the form of an optical fiber retaining the original glass transparency.[13] Bioresorbability is a step forward for safe and implantable optical devices that can be of great help in the reduction of medical costs and complexity of both the diagnosis and the therapy administration.[14] Such a fiber can be used to produce devices employed in several biomedical applications, from basic gas and liquid sensing[15–17] to *in vivo* imaging[18] and deep-tissue photodynamic therapy[19] as well as time-domain broadband diffuse optical spectroscopy.[20] Moreover, these glass compositions have been recently tested *in vivo*, to determine the biological response to fiber implantation,[21] and no clinical signs of any adverse effect were found in the tested animals. Mechanical behavior of these fibers has been tested both in form of core/cladding fibers and of capillaries.[22]

While showing good mechanical properties in the form of fibers, it is very difficult to realize complex preforms for capillaries and microstructured fibers based on these glasses through the conventional hole drilling techniques. To obtain capillaries, rotational casting technique can be used, while for microstructured fibers stack-and-draw of capillaries can be employed. However, rotational casting

has the limitation of the cylindrical shape of the preform and of its inner-to-outer diameter ratio, being at most 0.4÷0.6 for phosphate glasses.

The extrusion process is a well-known technique used for processing several materials. It consists of forcing a sufficiently soft material (i.e. a heated glass sample) through an orifice, namely a die, to impress a specified shape to the so-called extrudate. After passing through the die, the softened glass is cooled down to a temperature below its glass transition temperature, thus preserving the imposed shape. In all those applications where products with a fixed cross-sectional profile are required, the extrusion is perhaps the most suitable technique. Since the early '70s, studies have been published concerning the various applications of glass extrusion.[23] However, glass extrusion was seldom used, given the main focus on silica glasses and the good results of hole drilling in these materials. Nonetheless, glass extrusion has experienced a rebirth in recent years for the realization of either silicate or soft glass products especially employed in optical fiber fabrication. Several types of glasses (i.e. lead-silicate, tellurite, bismuth, fluoride, and phosphate) have been used within different extrusion systems, either for rod, core/cladding fibers, or for microstructured optical fibers.[24–35] Several studies have been published[29,34] on the application of the extrusion technique in the direct production of microstructured preforms, particularly with soft tellurite glasses[36] and either lead silicate glass, bismuth glass, or methacrylic polymer.[31] However, despite some great improvements both in the design of the preforms' shape and in the simplification of the whole process have been achieved, there are still several aspects to be addressed, mostly related to preform distortions. Models, as well as experimental tests, have been developed and the calculations seemed to be in good agreement with the actual results of performed extrusion, even in the presence of a high complexity die.[37–44] Despite the great advances highlighted in these works, there is still a lack of a fast and simple method capable of easily finding the main design parameters that would allow a smart die design and would minimize the undesired extrudate deviation from the ideal shape. Indeed, in several practical cases, a fast optimization cycle for die design is preferable to a more complex and rigorous mathematical model.

In the past 20 years, the fabrication of microstructured optical fibers has also gained increasing importance. These types of fibers can also be used for the production of photonic crystal fibers,[45–47] large mode area fibers,[48,49] high-resolution imaging[50] or supercontinuum generation,[51] and, in the form of hollow structures, are often employed as either gas or liquid sensors, due to the high surface area of interaction with the fluid medium.[52–54] Most of the listed applications could be applied inside the body, thus exploiting the possibility of realizing a microstructured fiber that is also bioresorbable. Nevertheless, the fabrication of a bioresorbable microstructured fiber has not been feasible so far due to the lack of a bioresorbable transparent glass and of more flexible fiber preform fabrication techniques.

In the present study, the behavior of bioresorbable phosphate glasses for the billet extrusion process, in view of obtaining complex preforms for optical fiber production, is reported. A fast and effective methodology for die optimization is presented employing basic fluid simulation.[55] Finally, microstructured fibers are realized by direct extrusion of the preform and by stack-and-draw of extruded capillaries.

Materials and methods

Phosphate glass fabrication and characterization

Bioresorbable phosphate glass samples were prepared by conventional melt-quenching technique, using chemicals with high purity level (>99%). Both weighing and mixing of the reagents were carried out within a dry box to minimize the hydroxyl ions (OH^-) content in the glass. The chosen glass composition (in mol%), derived from previous studies,[13] was 50% P_2O_5 – 23% MgO – 11.5% Na_2O – 10% CaO – 3% SiO_2 – 2.5% B_2O_3. The high amount of MgO, as already demonstrated, is able to lower the refractive index of the glass, providing at the same time a higher elastic modulus with respect to glasses with a lower MgO content.[22] Furthermore, even in the absence of special needs regarding the optical or mechanical properties of the glass, the choice of this composition has led to a worst-case scenario in terms of workability (i.e. difference between onset crystallization temperature T_x and glass transition temperature T_g of the material).

The prepared powder mixture was melted inside a furnace at a temperature of 1200 °C and then was cast into a preheated stainless-steel mold. The cast glass was subsequently annealed at a temperature close to the glass transition temperature, T_g, for a few hours, and finally slowly cooled to room temperature. The obtained glass billet showed a weight close to 45 g, a diameter of 25 mm, and a height ranging from 30 to 35 mm.

Glass fibers of the above-mentioned composition were tested for dissolution in a Phosphate Buffered Saline solution following the protocol detailed by Ceci-Ginistrelli *et al.*[13] to check their bioresorbability.

The viscosity measurement of the bioresorbable glass was carried out using a Thermo-mechanical analyzer (TMA, model SETARAM – SETSYS Evolution). The glass sample showed a cylindrical shape with a diameter of 4.22 mm and an initial height h of 5.38 mm. The sample was placed inside a stainless-steel container to avoid leakage during the test and a heating ramp of 5 °C/min under air flux was used. A weight M of 5 g was applied to the top of the sample and the piston displacement dh/dt was recorded during the whole instrument measurement range of 2 mm. The glass viscosity η has been calculated through the formula present in the ASTM Standard C1351M-96, that reads:

$$\eta = 2\pi \frac{Mgh^5}{30V(dh/dt)(2\pi h^3+V)(1+\alpha T)} \quad , \tag{1}$$

where V is the volume of the glass sample, α its coefficient of thermal expansion, and T the temperature. Due to the low α exhibited by the glass, namely $12.2 \cdot 10^{-6}$ K^{-1},[13] and after the ASTM Standard aforementioned, the term $(1+\alpha T)$ was neglected.

Simulation-aided die design

To model the flow behavior of the softened phosphate glass inside the extrusion die, a laminar incompressible fluid flow simulation has been carried out using the OpenFOAM® Computational Fluid Dynamics (CFD) toolbox provided by the SimScale open-source web platform.[55] The die design, realized with common Computer-Aided-Design (CAD) software, was used to calculate the shape of the fluid volume inside the die itself. By means of a Tet-dominant meshing algorithm,

integrated into the employed platform, a mesh of the fluid was constructed and refined along the solid-fluid boundaries. The applied model considered the laminar flow of a fluid with a kinematic viscosity of 4000 m^2/s, corresponding to the estimated viscosity of the glass during extrusion. The density of the fluid at the extrusion temperature was not available but the solid glass density was measured at room temperature according to Archimede's principle using distilled water as an immersion fluid. Considering several studies[56–58] where the density of different glass compositions was measured with respect to a huge range of temperature variation, the expected phosphate glass density reduction is less than 10% from room temperature to the softening temperature, which is an acceptable uncertainty given the complexity of the simulation where other factors could be of more influence than this variation. The glass temperature was assumed to be nearly constant inside the die, i.e. in the hot part of the extruder, thus a constant viscosity was employed for the calculations.

The calculations were computed with a no-slip condition over the die walls, i.e. the velocity of the fluid at the glass/wall boundary was set to zero and a velocity boundary condition was set up on the inlet (upper surface of the die), where the selected velocity is a mean value corresponding to an applied ram speed of 120 μm/min, characteristic of our extrusion process. Finally, a zero-gradient pressure surface was imposed on the outlet boundary (die exit) to account for free flow after extrusion.

The Newtonian behavior of the viscous glass flow is assumed in the presence of constant pressure, i.e. almost negligible strain-rate. In fact, a constant strain is the desired condition during extrusion to avoid differences in the stress-strain curves which are responsible for a non-Newtonian behavior.[59] However, this approximation is only possible in the central part of the extrusion process, i.e. in the region of constant force, which, indeed, is the one providing the useful portion of the extrudate.[40]

Extrusion

The home-built extruder used in this work and depicted in Fig. S1 is made of the following components: (i) an electrically heated furnace; (ii) a holding Inconel (Nickel-based alloy) cylinder, which is used to support (iii) the die (made of AISI 304 stainless steel); (iv) the glass billet, which is the last fixed element of the extruder; furthermore, (v) the stainless steel ram connected to (vi) the

driving motor (MAXON brushless DC motor), which are the moving parts of the system; those latter elements allow the softened glass to be forced to pass through the die; the furnace temperature is constantly measured using (vii) a thermocouple placed in contact with the die base; also the applied force is controlled by means of (viii) a load cell placed between the ram and the motor. The extrusion force can vary up to 5000 N and is determined based on the die shape and the glass characteristic temperatures, with typical values of 1000 N.

Microstructured fiber drawing

Several extrusion dies were employed to produce preforms with different diameters and shapes. Cylindrical preforms were realized with different dies showing outer diameters of 10 and 12 mm and inner diameters of 6 and 8 mm. The preform with the highest internal diameter was employed to produce the outer cladding of the fiber, while the one with a smaller hole was subsequently stretched to form the inner tubes of the microstructured fiber.

The microstructured fiber was drawn from a preform made of a stack of the extruded samples. The preform assembly was carried out in a controlled atmosphere, to minimize the contamination. The stretched tubes were all selected to show nearly the same diameter (corresponding to 850 ± 5 μm); in fact, even small differences in the diameter of the tubes would lead to the misalignment of the stacking. A full bundle of the selected tubes, with a solid core at its center, was inserted into the bigger extruded tube. The obtained preform was finally mounted into an *in-house* developed drawing tower, where an induction heating ring (SAET, Torino, Italy), operating at 248 kHz and delivering 170 W, was used to reach the drawing temperature. The drawing tower parameters were set to obtain a microstructured fiber having an outer diameter of 125 μm, to match one of the most common standards related to fiber dimensions for optics and telecom applications.

With the perspective to realize more complex multifunctional optical fibers and to further investigate the flow behavior of the glass in the presence of different diameters holes, a double-core die was designed and manufactured, with two different pins with a diameter of 1.5 and 3 mm, respectively.

Results and discussion

The path toward the direct preform extrusion and microstructured fiber drawing of bioresorbable calcium-phosphate glass is based on three main processes: glass billet fabrication, extrusion through a suited die, and fiber drawing. In this work, all three phases have been investigated to demonstrate: optimal glass properties, a method for die optimization with the support of numerical modeling, and the fabrication of a microstructured optical fiber. The bioresorbable glass used in the present work contains 50 mol% of P_2O_5, which favors the presence of a polymeric-like network that helps the glass to be drawable.[12,60] Detailed study of the composition, together with its dissolution properties, was performed by Ceci-Ginistrelli *et al.*[13] In terms of optical properties, the glass displayed a wide optical window, i.e. an UV-edge of 240 nm, and optical transparency extended toward NIR wavelengths (> 2500 nm) with no absorption peaks. The most relevant properties of the fabricated glass are reported in Table 1 for the sake of completeness.

Table 1. Manufactured phosphate glass properties: glass transition temperature T_g, onset crystallization temperature T_x, working temperature range ΔT (i.e. the difference between onset crystallization and glass transition temperatures), glass density ρ, elastic modulus E, transparency window TW, and refractive index n measured at a wavelength of 633 nm.

	T_g [°C]	T_x [°C]	ΔT [°C]	ρ [g/cm^3]	E [GPa]**	TW [nm]*	n*
Glass	477 ± 3	625 ± 3	148 ± 6	2.589 ± 0.005	51.1 ± 0.9	240 ÷ 2500	1.52 ± 0.001

* data from Ceci-Ginistrelli *et al.*[13]

** data from Sglavo *et al.*[22]

The chosen composition showed good workability which originates from the distance between the glass transition temperature T_g and the onset crystallization temperature T_x. The viscosity curve of the glass fabricated by melt-quenching was measured to obtain reference temperatures and viscosities to be used during the extrusion process and the results are shown in Fig. 1. Such glass presents a working temperature range of 517-552 °C, corresponding to viscosities of 10^8-$10^{6.5}$ Pa·s.

The glass was then cast into billets of cylindrical shape with heights of about 35 mm and diameters of 25 mm, which were used for the extrusion of the tubes and complex preforms. Extrusions of tubes showing different inner (ID) and outer (OD) diameters were used to test the process conditions and as a benchmark of the modeling tools. Indeed, the tubes showing an ID/OD equal to 8/10 allow to overcome the limitation of preform fabrication technology for the bioresorbable glass introduced by rotational casting technique.

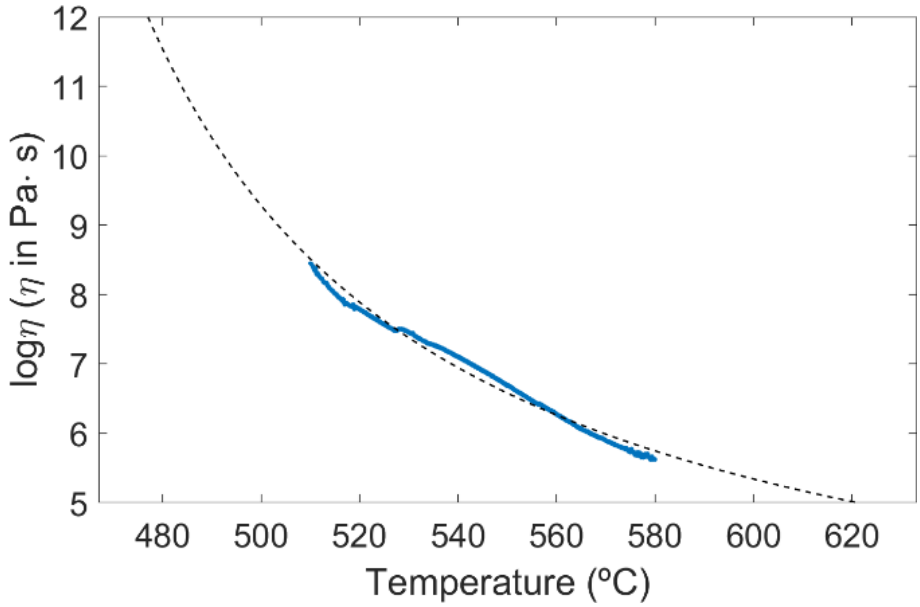

Figure 1. Viscosity curve of the bioresorbable glass as obtained through the TMA measurement. The blue line indicates the experimental data, while the dashed line is the log fitting of the viscosity curve.

The extrusion of such tubes was realized at a temperature of 540 °C (nominal viscosity of 10^7 Pa·s) with a force of 800 N. The ram speed was controlled during extrusion and was set mostly at 120 µm/min. A typical extruded tube is shown in Fig. 2a, where three regions can be identified: *(i)* the initial bending region, *(ii)* one region usable for preform making, and *(iii)* the neck-down region.

The first region is typical of the extrusion process and can be related to e.g. slight asymmetries in the applied ram pressure (see SI for further considerations on preform bending). After the first initial region, the extrusion transitions to a straighter and more usable region that is the one that is cut and employed as a preform. The final neck-down region is induced by an increase in temperature (up to 575 °C) to stop the extrusion and let the tube be removed from the extruder by the operator. The

roughness of the produced tubes was also measured in the inner surface of the tube and the results are reported in Fig. S2 giving an overall roughness of $R_a = 0.37$ nm, which is comparable to the one obtained with commercially available glasses. Moreover, as reported in Fig. 2b-c, the usable section of a tube was stretched in the form of capillaries and stacked in another extruded tube to make the preform of a microstructured fiber.

To develop a model that could be used as a tool for die optimization, extrusion of tubes through the used dies was computed.

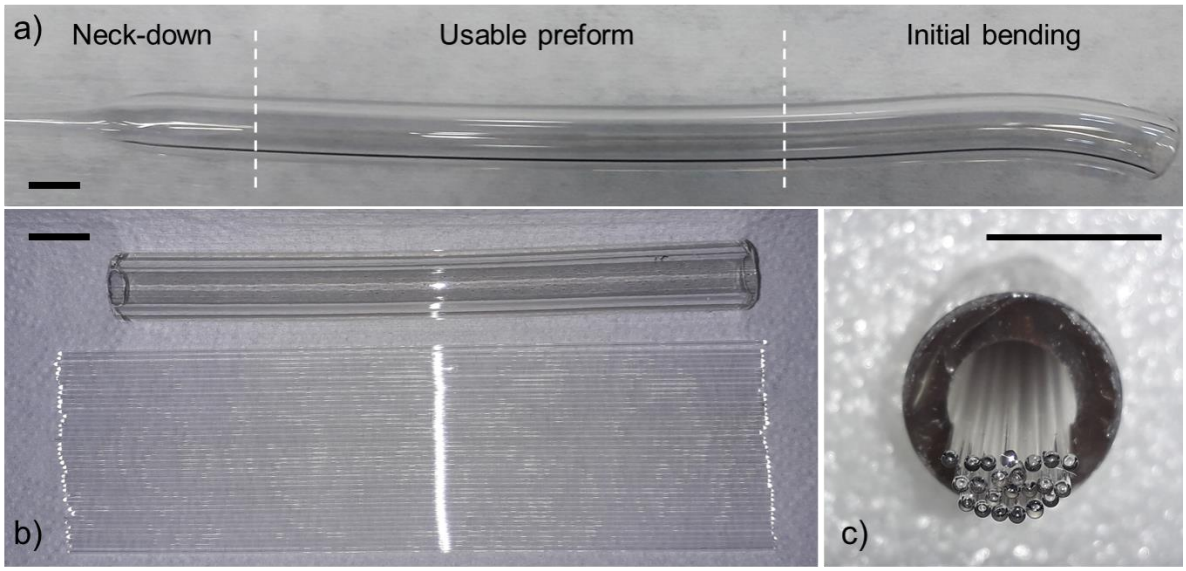

Figure 2. (a) Pictures of a complete extruded tube with highlighted the three main regions of the extrudate (i.e. the initial bending, the useful region, and the final neck-down). (b) Outer (top) and inner (bottom) samples employed for the manufacturing of the microstructured fiber. (c) An intermediate step during the stacking of capillaries. All the scale bars are equal to 10 mm.

The simulation focuses on the viscous flow of the bioresorbable glass inside the die and predicts the shape and velocity at the die exit. To keep the model simple and useful as a die design support tool, some approximations have been used. Indeed, no deformation due to gravity, i.e slenderness, was considered since it could be sufficiently controlled if the temperature inside the die is kept around the softening point of the specific glass, thus by extruding at high viscosities. The complex phenomenon of die swelling, i.e. the enlargement of the extrudate's shape after the passage through the die, carefully modeled by Mayer *et al.*[61] and subsequently by Trabelssi *et al.*,[41] was also neglected in the

present work. Although the swelling effect cannot be removed at all but simply limited by reducing the friction at the glass/die interface, it does not significantly influence the flow inside the die but causes a dimensional growth of the features of the glass preform. If precise tube dimensions are required, the amount of these distortions can be taken into account as detailed by Kalnins *et al.*[62] In our case, both the temperature control, which influences the glass viscosity, and the weight of the extrudate due to the relatively low glass density (compared to other glass systems)[63] as well as the preform dimensions, led to homogenous and controllable distortions in the extruded products.

An example result of the simulation of the flow through a die for tube extrusion is reported in Fig. S3 and can be compared with the portion of the tube in Fig. 2b, which is the usable region of the extrudate reported in Fig. 2a. The numerical results show flow velocities that are in good agreement with the ones of the glass outside the extruder measured during the experiment, which were about 1.1 mm/min. To demonstrate the use of such numerical tool in the design of a preform, different die shapes were also designed to produce double-core preforms, having a couple of different blocking elements (with a diameter of 3 and 1.5 mm, respectively), thus breaking the circular symmetry of the die with the aim of producing a multi-core preform.

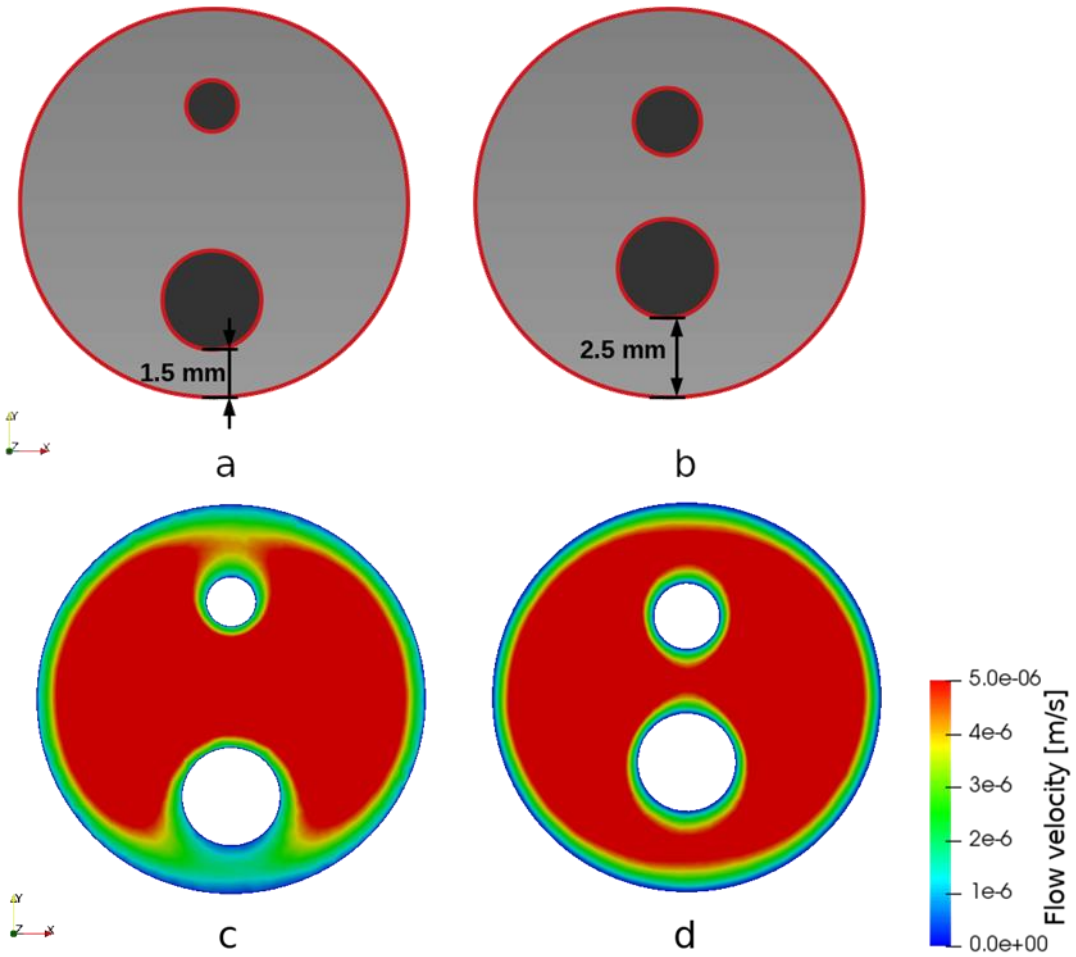

Figure 3. Detailed sections of the manufactured dies and results of the flow simulation. Sketch of the section of the first die (a) and of the optimized die (b); the dark-grey areas represent the blocking elements or the holes of the preform, while the remaining light-grey area represents the glass portion of the preform. Result of the simulation of the softened glass flow velocity at the die exit for (c) configuration a) and (d) for configuration b) designs.

The first design of such a die is sketched in Fig. 3a. The simulated flow at the exit of the die is reported in Fig. 3c and shows a serious flow reduction between the blocking elements and the walls of the die. This behavior is confirmed by the experimental results shown in Fig. 4a, where the double-core preform is compared with the cross-section of the die sketched in Fig. 3a. The reduced flow in the simulations experimentally corresponds to a lack of material (particularly visible in the upper part of Fig. 4a, thus explaining the deformation of the extrudate. To solve this issue, the die shape has been redesigned reducing the gap between the two blocking elements, both in terms of the distance between the elements and of their relative dimensions. The new die design, depicted in Fig. 3b, shows two

blocking elements with diameters of 3 and 2 mm and a distance between the pins and the die wall of 2.5 mm (i.e. 1 mm higher than the original one). For the sake of completeness, the preform obtained with the optimized die is reported in Fig. 4b, highlighting the better homogeneity of the glass distribution all over the section of the preform. However, also the swelling phenomenon is slightly more evident in this latter configuration and leads to a nearly uniform variation of the preform dimensions with respect to the die geometry.[43,44] A further optimization of the die design can take the swelling into account and compensate for it.

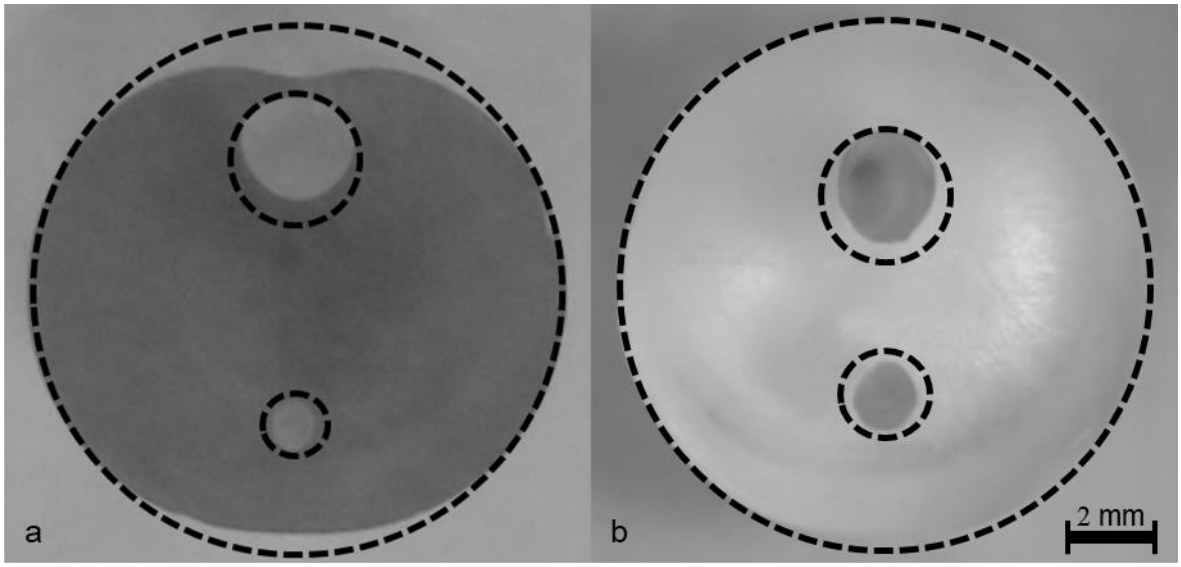

Figure 4. Section of the produced preforms made with (a) the first die and (b) the optimized die. The dashed line corresponds to the geometry of the dies reported in Figs. 3a and b.

The section of the computed glass flow is shown in Fig. 3d. With this configuration, a more homogeneous flow distribution could be obtained over the whole section of the die. The model does not take into account holes distortion, which indeed could be derived by the gradient of the actual glass distribution over the whole section. Although possible, this complicates the whole approach and the calculations could be developed in a future optimization step.

To demonstrate the fabrication of a microstructured fiber with the extruded bioresorbable glass, some of the tubes were stretched to form small capillaries which were subsequently stacked together in a bundle (see Fig. 2c). The capillaries were stretched to have an outer diameter of 850 μm. The

manufactured bundle was composed of 42 hollow elements with the addition of a central all-solid core. The bundle was then inserted into another extruded tube and the capillaries were sealed on both sides by quickly heating their extremity with a flame. The assembled preform was thus drawn into the microstructured fiber, whose section is shown in Fig. 5. The fiber cross-section was checked at regular intervals of about 10 m over the span of the drawn fiber and the geometry was found to be conserved along all this length. Several tens of meters of microstructured optical fibers were produced, demonstrating the viability of the process and paving the way for bioresorbable photonic crystal fiber production. Further studies regarding the characterization of the optical properties of the fiber as well as the thorough optimization of the process are ongoing and will be reported soon.

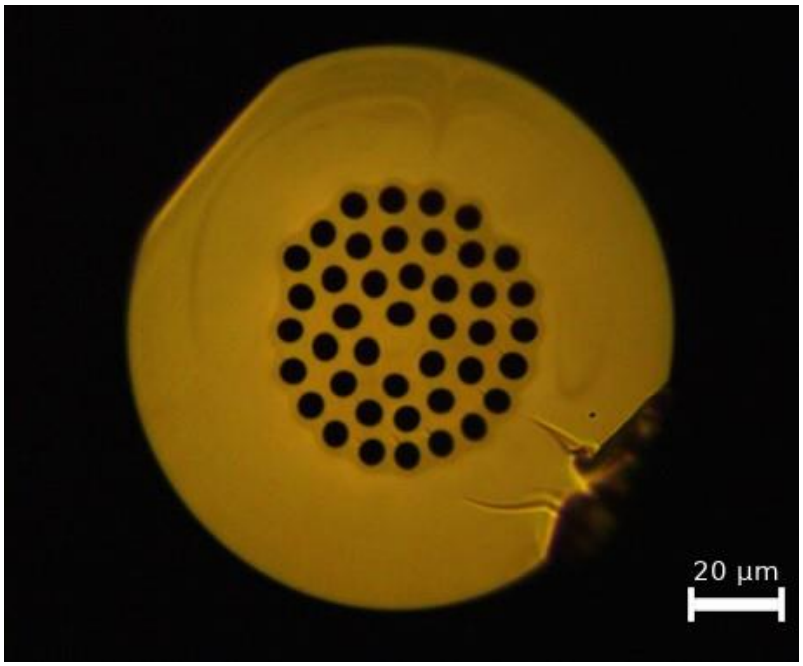

Figure 5. Cross-section of the bioresorbable phosphate glass-based microstructured fiber.

Conclusions

In the present work, the whole process employed to fabricate a microstructured optical fiber via extrusion of a bioresorbable phosphate glass has been carefully analyzed. Starting from glass manufacturing and characterization, it was demonstrated the applicability of extrusion of custom-made bioresorbable glasses in the manufacturing of tubes for fiber preforms. A simple computational tool to support die design has been developed and tested against the extrusion of single tubes and of

more complex double-core geometries. To overcome the limitations exhibited by common preform fabrication techniques usable with the bioresorbable glass presented, extrusion is a crucial step, in particular for the production of complex-shaped fibers. To support the complex task of die design a simulation-aided approach was introduced. This approach could encourage a true step forward leading in the near future to the fabrication of a directly extruded microstructured bioresorbable phosphate glass fiber preform. In addition, extruded tubes have been successfully used to produce a microstructured bioresorbable phosphate glass fiber obtained via the stack-and-draw technique, thus opening new possibilities for this glass in terms of fabrication and potential applications.

Acknowledgments

The authors would like to thank the Interdepartmental Center PhotoNext of Politecnico di Torino for its support. Dr. M. Facciano and Mr. F. Strata are also warmly acknowledged for their respective help in the manufacturing of the fiber via the stack-and-draw technique and in carrying out the computational simulations. The authors acknowledge help received by Dr. G. Marchese for TMA measurements and by prof. R. Gonnelli and Dr. E. Piatti for AFM measurements. D. Janner acknowledges financial support from Compagnia di S. Paolo through the Starting Grant Program.

References

1. Boetti N, Pugliese D, Ceci-Ginistrelli E, Lousteau J, Janner D, Milanese D. Highly doped phosphate glass fibers for compact lasers and amplifiers: a review. Appl Sci 2017;7(12):1295.
2. Pugliese D, Boetti NG, Ceci-Ginistrelli E, et al. Multicomponent rare earth-doped phosphate glasses for compact lasers and amplifiers. Proceedings of the 20th International Conference on Transparent Optical Networks; 2018 July 1-5; Bucharest, Romania. New York:IEEE; 2018.
3. Hoppe A, Güldal NS, Boccaccini AR. A review of the biological response to ionic dissolution products from bioactive glasses and glass-ceramics. Biomaterials 2011;32(11):2757–2774.
4. Baino F, Hamzehlou S, Kargozar S. Bioactive glasses: where are we and where are we going? J Funct Biomater 2018;9(1):25.
5. Baino F. Bioactive glasses – When glass science and technology meet regenerative medicine. Ceram Int 2018;44(13):14953–14966.
6. Moss RM, Pickup DM, Ahmed I, Knowles JC, Smith ME, Newport RJ. Structural characteristics of antibacterial bioresorbable phosphate glass. Adv Funct Mater 2008;18(4):634–639.

7. Ahmed I, Lewis M, Olsen I, Knowles, JC. Phosphate glasses for tissue engineering: Part 2. Processing and characterisation of a ternary-based P_2O_5-CaO-Na_2O glass fibre system. Biomaterials 2004;25(3):501–507.

8. Massera J, Ahmed I, Petit L, Aallos V, Hupa L. Phosphate-based glass fiber vs. bulk glass: Change in fiber optical response to probe in vitro glass reactivity. Mater Sci Eng, C 2014;37:251–257.

9. Massera J, Shpotyuk Y, Sabatier F, et al. Processing and characterization of novel borophosphate glasses and fibers for medical applications. J Non-Cryst Solids 2015;425:52–60.

10. Abou Neel EA, Pickup DM, Valappil SP, Newport RJ, Knowles JC. Bioactive functional materials: a perspective on phosphate-based glasses. J Mater Chem 2009;19:690–701.

11. Brow RK. Review: the structure of simple phosphate glasses. J Non-Cryst Solids 2000;263–264:1–28.

12. Knowles JC. Phosphate based glasses for biomedical applications. J Mater Chem 2003;13(10):2395–2401.

13. Ceci-Ginistrelli E, Pugliese D, Boetti NG, et al. Novel biocompatible and resorbable UV-transparent phosphate glass based optical fiber. Opt Mater Express 2016;6(6):2040–2051.

14. Shin J, Yan Y, Bai W, et al. Bioresorbable pressure sensors protected with thermally grown silicon dioxide for the monitoring of chronic diseases and healing processes. Nat Biomed Eng 2019;3(1):37–46.

15. Cubillas AM, Unterkofler S, Euser TG, et al. Photonic crystal fibres for chemical sensing and photochemistry. Chem Soc Rev 2013;42(22):8629–8648.

16. Mishra A, Désévédavy F, Petit L, Smektala F, Massera J. Core-clad phosphate glass fibers for biosensing. Mater Sci Eng, C 2019;96:458–465.

17. Lopez-Iscoa P, Ojha N, Pugliese D, et al. Design, processing, and characterization of an optical core-bioactive clad phosphate fiber for biomedical applications. J Am Cer Soc 2019;102(11):6882–6892.

18. Nazempour R, Zhang Q, Fu R, Sheng X. Biocompatible and implantable optical fibers and waveguides for biomedicine. Materials 2018;11(8):1283.

19. Dougherty TJ, Gomer CJ, Henderson BW, et al. Photodynamic therapy. J Natl Cancer Inst 1998;90(12):889–905.

20. Di Sieno L, Boetti NG, Dalla Mora A, et al. Towards the use of bioresorbable fibers in time-domain diffuse optics. J Biophotonics 2018;11(1):e201600275.

21. Podrazký O, Peterka P, Kašík I, et al. In vivo testing of a bioresorbable phosphate-based optical fiber. J Biophotonics 2019;12(7):e201800397.

22. Sglavo VM, Pugliese D, Sartori F, et al. Mechanical properties of resorbable calcium-phosphate glass optical fiber and capillaries. J Alloys Compd 2019;778:410–417.

23. Roeder E. Extrusion of glass. J Non-Cryst Solids 1971;5(5):377–388.

24. Seddon AB, Furniss D, Motesharei A. Extrusion method for making fiber optic preforms of special glasses. Proceedings of SPIE Conference on Infrared Glass Optical Fibers and Their Applications; 1998 July 13-16; Québec, Canada. Bellingham:SPIE; 1998. p. 32–42.

25. Furniss D, Seddon AB. Towards monomode proportioned fibreoptic preforms by extrusion. J Non-Cryst Solids 1999;256–257:232–236.

26. Bhowmick K, Morvan HP, Furniss D, Seddon AB, Benson TM. Co-extrusion of multilayer glass fiber-optic preforms: prediction of layer dimensions in the extrudate. J Am Ceram Soc 2013;96(1):118–124.

27. Petropoulos P, Ebendorff-Heidepriem H, Finazzi V, et al. Highly nonlinear and anomalously dispersive lead silicate glass holey fibers. Opt Express 2003;11(26):3568–3573.

28. Ebendorff-Heidepriem H, Petropoulos P, Asimakis S, et al. Bismuth glass holey fibers with high nonlinearity. Opt Express 2004;12(21):5082–5087.

29. Feng X, Monro TM, Finazzi V, et al. Extruded singlemode, high-nonlinearity, tellurite glass holey fibre. Electron Lett 2005;41(15):835–837.

30. Lee ETY, Taylor ERM. Two-die assembly for the extrusion of glasses with dissimilar thermal properties for fibre optic preforms. J Mater Process Technol 2007;184(1–3):325–329.

31. Ebendorff-Heidepriem H, Monro TM. Extrusion of complex preforms for microstructured optical fibers. Opt Express 2007;15(23):15086–15092.

32. Ebendorff-Heidepriem H, Warren-Smith SC, Monro TM. Suspended nanowires: fabrication, design and characterization of fibers with nanoscale cores. Opt Express 2009;17(4):2646–2657.

33. Leong JYY, Petropoulos P, Price JHV, et al. High-nonlinearity dispersion-shifted lead-silicate holey fibers for efficient 1-μm pumped supercontinuum generation. J Light Technol 2006;24(1):183–190.

34. Kumar VVRK, George AK, Knight JC, Russell PSJ. Tellurite photonic crystal fiber. Opt Express 2010;11(20):2641–2645.

35. Tsiminis G, Rowland KJ, Schartner EP, Spooner NA, Monro TM, Ebendorff-Heidepriem H. Single-ring hollow core optical fibers made by glass billet extrusion for Raman sensing. Opt Express 2016;24(6):5911–5917.

36. Oermann MR, Ebendorff-Heidepriem H, Ottaway DJ, Lancaster DG, Veitch PJ, Monro TM. Extruded Microstructured Fiber Lasers. IEEE Photon Technol Lett 2012;24(7):578–580.

37. Xue SC, Tanner RI, Barton GW, Lwin R, Large MCJ, Poladian L. Fabrication of microstructured optical fibers - Part I: problem formulation and numerical modeling of transient draw process. J Light Technol 2005;23(7):2245–2254.

38. Xue SSC, Tanner RI, Barton GW, Lwin R, Large MCJ, Poladian L. Fabrication of microstructured optical fibers - Part II: numerical modeling of steady-state draw process. J Light Technol 2005;23(7):2255–2266.

39. Kostecki R, Ebendorff-Heidepriem H, Warren-Smith SC, Monro TM. Predicting the drawing conditions for Microstructured Optical Fiber fabrication. Opt Mater Express 2014;4(1):29–40.

40. Ebendorff-Heidepriem H, Monro TM. Analysis of glass flow during extrusion of optical fiber preforms. Opt Mater Express 2012;2(3):304–320.

41. Trabelssi M, Ebendorff-Heidepriem H, Richardson KA, Monro TM, Joseph PF. Computational modeling of hole distortion in extruded microstructured optical fiber glass preforms. J Light Technol 2015;33(2):424–431.

42. Tronnolone H, Stokes YM, Foo HTC, Ebendorff-Heidepriem H. Gravitational extension of a fluid cylinder with internal structure. J Fluid Mech 2016;790:308–338.

43. Trabelssi M, Joseph PF. Hole distortion and drift in extruded microstructured optical fiber glass preforms: Part I – Sensitivity analysis. J Non-Cryst Solids 2018;481:208–224.

44. Trabelssi M, Joseph PF. Hole distortion and drift in extruded microstructured optical fiber glass preforms: Part II – Optimization. J Non-Cryst Solids 2018;481:412–423.

45. Knight JC. Photonic crystal fibres. Nature 2003;424:847–851.

46. Rifat AA, Hasan MdR, Ahmed R, Butt H. Photonic crystal fiber-based plasmonic biosensor with external sensing approach. J Nanophotonics 2017;12(1):012503.

47. Rifat AA, Ahmed R, Yetisen AK, et al. Photonic crystal fiber based plasmonic sensors. Sens Actuators B Chem 2017;243:311–325.

48. Li L, Schülzgen A, Temyanko VL, et al. Short-length microstructured phosphate glass fiber lasers with large mode areas. Opt Lett 2005;30(10):1141–1143.

49. Feng X, Flanagan JC, Frampton KE, et al. Single-mode tellurite glass holey fiber with extremely large mode area for infrared applications. Proceedings of the 2008 Conference on Optical Fiber Communication/National Fiber Optic Engineers Conference (OFC/NFOEC 2008); 2008 February 24-28; San Diego, USA. New York:IEEE; 2008.

50. Warren-Smith SC, Dowler A, Ebendorff-Heidepriem H. Soft-glass imaging microstructured optical fibers. Opt Express 2018;26(26):33604–33612.

51. Cassataro M, Novoa D, Günendi MC, et al. Generation of broadband mid-IR and UV light in gas-filled single-ring hollow-core PCF. Opt Express 2017;25(7):7637–7644.

52. Cox FM, Argyros A, Large MCJ. Liquid-filled hollow core microstructured polymer optical fiber. Opt Express 2006;14(9):4135–4140.

53. Skorobogatiy M. Microstructured and photonic bandgap fibers for applications in the resonant bio- and chemical sensors. J Sens 2009;2009:524237.

54. Fini JM, Nicholson JW, Mangan B, et al. Polarization maintaining single-mode low-loss hollow-core fibres. Nat Commun 2014;5:5085.

55. http://www.simscale.com

56. Bottinga Y, Richet P, Weill DF. Calculation of the density and thermal expansion coefficient of silicate liquids. Bull Minéral 1983;106(1):129–138.

57. Shartsis L, Spinner S. Viscosity and density of molten optical glasses. J Res Natl Bur Stand 1951;46(3):176–194.

58. Napolitano A, Macedo PB, Hawkins EG. Viscosity and density of boron trioxide. J Am Ceram Soc 1965;48(12):613–616.

59. Simmons JH, Mohr RK, Montrose CJ. Non-Newtonian viscous flow in glass. J Appl Phys 1982;53(6):4075–4080.

60. Sharmin N, Parsons AJ, Rudd CD, Ahmed I. Effect of boron oxide addition on fibre drawing, mechanical properties and dissolution behaviour of phosphate-based glass fibres with fixed 40, 45 and 50 mol% P_2O_5. J Biomater Appl 2014;29(5):639–653.

61. Mayer H-J, Stiehl C, Roeder E. Applying the finite-element method to determine the die swell phenomenon during the extrusion of glass rods with non-circular cross-sections. J Mater Process Technol 1997;70(1–3):145–150.

62. Kalnins CAG, Bachus KJ, Gooley A, Ebendorff-Heidepriem H. High precision extrusion of glass tubes. Int J Appl Glass Sci 2019;10(2):172–180.

63. Bach H, Neuroth N. The Properties of Optical Glass; Springer-Verlag: Berlin Heidelberg; 1998.